IIETA International Information and Engineering Technology Association
Advancing the World of Information and Engineering

Mathematical Modelling of Engineering Problems
Vol. 12, No. 10, October, 2025, pp. 3493-3509
Journal homepage: http://iieta.org/journals/mmep

Numerical Investigation of Web Opening Composite Beams Made with Y-Rib Shear Connectors

Ali Habeeb Noori*, Abdulnasser M. Abbas

Civil Engineering Department, College of Engineering, University of Basra, Basra 61001, Iraq

Corresponding Author Email: pgs.ali.habeeb@uobasrah.edu.iq

https://doi.org/10.18280/mmep.121016

Received: 5 June 2025
Revised: 19 August 2025
Accepted: 25 August 2025
Available online: 31 October 2025

Keywords:
composite beams, shear stud connector, Y-rib connector, web opening, failure mode, structural behaviour, bond slippage

ABSTRACT

Composite steel-concrete beams are widely used in buildings and bridges due to their nature, ease of construction, low cost, and excellent structural performance. Ventilation ducts and pipes under beams in high-rise buildings restrict floor clearance. Composite steel-concrete beams with web openings can overcome the above-mentioned impediments but have lower flexural strength and load-carrying capacity. This study presents the numerical investigation of the shear behavior of steel-concrete composite beams. In this study, steel-concrete composite beams were constructed with a welded steel I-section beam and concrete slab with different shear connections. Twelve simply supported composite beams subjected to two-point concentrated loads were numerically tested. Three variables were considered: the connection ratios, which were taken as 100%, 70%, and 50%; the types of shear connectors; and the presence of web openings. A numerical analysis was also conducted to assess whether the beam behavior could be simulated in the commercial finite element code ABAQUS. The study outcomes were the deflection at the mid-span of the beam, the cracking load, the bond slip, the crack pattern, the failure mode, and the slip mode. The main results indicate that the ultimate load capacity of Y-rib connection beams, increased by approximately 1.88%, 2.28%, and 3.215% for connection ratios of 50%, 70%, and 100%, respectively, compared to bolt stud beams. Conversely, the mid-span deflection of the Y-rib tested beams increased by approximately 104.33%, 94.25%, and 57.98%, respectively, compared to the reference beams. In comparison to the reference specimens, the connections ratio (shear connectors spacing) showed that the combined effect of prefabricated composite specimens reduces as the distance of the studs increases. On the other hand, the analysis indicates that stiffness and ultimate capacity are significantly reduced after a web opening under a negative bending moment. However, the main failure mode observed in all composite beam specimens was shear failure.

1. INTRODUCTION

The steel-concrete composite beam is one of the most widely used structural forms in large span structures and high-rise buildings. Composite steel-concrete beams offer a synthesis of durability, rigidity, design flexibility, stiffness, and cost efficiency, making composite structure a popular decision for several significant construction works. Initially, the typical composite beam model is the steel I-shape section connected together with a concrete slab or a profiled steel-concrete composite slab. These materials produce a structural system that is both economical and effective by combining the compressive strength and rigidity of concrete with the tensile strength of steel section [1]. In this case, the concrete block mainly experiences compressive forces, whereas the steel beam experiences tension stress, thus utilizing the beneficial characteristics of each material [2-4]. To allow this composite action, however, a shear connection between the concrete slab and the steel section must be properly designed. Since the early 20th century, researchers have used mechanical shear connectors to create shear connections to steel-concrete beams. Numerous types of shear connector types, including oscillating perfobond strips, waveform strips, headed studs, perfobond ribs, t-rib connectors, channel connectors, and non-welded connectors, have been used in composite beams [5].

Welded stud connectors have become the most popular type of mechanical shear connector used in composite floor systems in the construction industry. The availability of detailed research [6-10] and standard design methods have made welded studs very popular. Marshall et al. [11] conducted a number of reinforced composite beam studies, including push-out tests utilizing high-strength bolts in place as welded studs. Kwon et al. [12, 13] examined an experiment utilizing the mentioned high-strength bolts for shear connectors. The research found that all three types of high-strength bolts had superior fatigue properties relative to the welding shear studs typically used in practice. Lam and Saveri [14] and Pavlović et al. [15] used welded shear studs and different kinds of bolted connections to do push tests and look at how bolted connectors behave differently than welded stud

connectors. Moynihan and Allwood [16] evaluated three composite concrete specimens of different lengths (2, 5, and 10 m), fabricated using M20 bolts as separable shear connections. The findings showed that tested reinforced composite beams with bolted connectors have the same moment capacity as tested composite beams with welded shear studs. Mirza et al. [17] performed initial push-test studies with blind bolts. Experimental results indicate that these bolted connections exhibit similar performance and the capacity of welding head shear connections.

On the other hand, the research of composite beams with web openings has also been concerned by researchers and a remarkable progress has been made in the aspect of welded studs connected composite beams with web openings. Darwin and Donahey [18] presented generally design methods to calculate composite beams with rectangular web openings, which were easier and were in good agreement with test results. Liao et al. [19] conducted a series of nonlinear analysis on composite beams with rectangular web openings using ANSYS packages. The construction loads had no obvious influence on unshored construction when the loads did not exceed 60% of the non-composite beam resistance. Ataei et al. [20] performed experimental studies and finite element simulations on composite beams using high-strength bolts as shear connectors, but their research mostly focused on prefabricated steel geopolymer concrete (GPC) composite beams.

Thus far, some calculation methods have been presented for predicting the load carrying capacity of the composite beams with web openings [21-25]. The structural performance of the reinforced composite specimens containing openings during the test was simulated by three-dimensional finite element modeling. The behavior of the concrete was modeled by defining damage criteria utilizing the concrete damage plasticity (CDP) application in ABAQUS finite element software. Researchers have conducted several experimental and theoretical studies on the structural behavior of composite beams containing web openings over the past thirty years [26-33]. Redwood and Pournbouras [34], Clawson and Darwin [35], and Chung and Lawson [36] investigated the influence of opening location, opening form, and bending shear ratio on the structural properties of composite beams with web openings subjected to normal bending moments by experimental methods. Liao et al. [19] performed a nonlinear analysis of RC composite beams including rectangular web holes utilizing ANSYS software. Li et al. [37] presented the experimental findings of six continuous composite beams including rectangular web holes. However, most of the available investigations were predicated on cast-in-situ steel-concrete beams employing conventionally welded shear studs as shear connections. Clawson and Darwin [21] performed bending tests for six composite concrete specimens with rectangle web openings and one steel beam to examine moment-shear ratios that vary from 0.9 to 10 m. The failure mechanism of tested samples that had lower moment-shear ratios contained the creation of plastic hinges in the metal web opening and diagonal tension collapse of the concrete block. Redwood and Poumbouras [23] studied the significance of shear connections about the length of web openings and the impact of unshored structures. The results of the study indicated that a high shear-to-moment ratio during loading extensively influenced the load-carrying capacity due to a small shear connection in the web opening length. Park et al. [26] observed that the failed mechanism of the concrete block depends on the slab thickness. The composite-tested concrete specimens with a wide slab exhibited pullout failures at the shear connections, whereas those with a small slab width experienced diagonal tension failure on the concrete block. Ellobody et al. [32] conducted using finite element analysis on composite tested specimens with both stiffened and unstiffened web openings. When compared to composite beams with web holes that weren't stiffened, the research showed that composite beams with horizontal stiffeners were much better at carrying weight. The research results indicate that bolted shear-connected composite beams with web openings may have comparable mechanical properties to cast-in-situ welded stud-connected composite beams.

It can be observed from the previously mentioned studies that very few numerical studies have performed the structural behavior of opening composite steel-concrete beams with shear studs and Y-rib connections. Therefore, further numerical investigations are required in this area. In this paper, a numerical model is then developed and analyzed for composite beams with web openings under shear failure mode. The main parameters in this work are the shape of the opening, the size of the opening, the location of the opening, and the types of shear connectors. Two types of shear connectors, including bolt studs and Y-shaped connectors were used. The finite element models have been verified by comparing the load-deflection response results from prior experimental and simulated research. Three-dimensional non-linear models with finite element methods (FEMs) were created utilizing ABAQUS to replicate the examined composite beams. Also, the slip between the concrete block and the I-steel beam of the tested composite specimens at the interface was analyzed using FEMs. The failure modes, ultimate failure load, crack pattern concrete slab, ultimate shear capacity, cracking load, load-deflection, and load-slip curves were investigated.

2. NUMERICAL MODEL

2.1 Material modelling

In ABAQUS program, the material specifications data are entered in stages according to the behavior of the material where the first stage is elasticity and then the plasticity stage. For elastic stage passion ratio and elasticity modulus for material are used in the present analysis. For plasticity, ABAQUS provides several models depending on the material behavior after elastic stage. In present analysis, Concrete Damaged Plasticity (CDP) model is utilized in this research to resemble the response of normal concrete up to failure. In this model, the main mechanisms of concrete failure are tensile cracking and crushing. In the other hand, Smeared Cracking Model applied with ABAQUS/Standard and offers significant simplifications for concrete structures which are supposed to represent compressive crushing or tensile cracking. While, a Brittle Cracking Model is used for structures under dynamic load and it is only available in ABAQUS/Explicit. Generally, concrete is simulated as a homogeneous material. In the current model, many of the necessary plasticity parameters for the RC slab were left at ABAQUS's default settings. However, the CDP incorporates several variables, some derived from experimental testing. To account for the elastic stage, the Poisson ratio and the material's elasticity modulus have been used. On the other hand, for the plasticity stage, ABAQUS presents numerous models based on the material's behavior

after the elastic stage. The required plasticity parameters for the CDP model in ABAQUS are: (1) Dilation angle (ψ), is a material parameter determined at a high confining pressure in confining pressure (p) and von Mises stress (q) plane and indicates the inclination of an incremental plastic strain. ψ has a maximum value of 56.30 and a minimum value is approximately 00. Upper values are more ductile behavior, whereas lower values are more brittle. Based on Pan et al. [38], more agreement has been obtained with the experimental results for dilation angles between 30 and 40; for standard concrete, ψ equal to 30 is considered adequate. (2) Eccentricity (Є): defines the change rate of plastic flow potential function. In ABAQUS 0.1 can be considered as the eccentricity default value, where the dilation angle has no change for a wide range of confining pressure. For low confining pressure a higher eccentricity value than 0.1 induces a rapid increase in the dilation angle. Although a lower value than 0.1 will cause a problem of convergence when the material is submitting to the low values of confining pressure. (3) σ_{bo}/σ_{co}: refers to the ratio of initial equibiaxial compressive yield stress to initial uniaxial compressive yield stress. In the present study the value 1.16 was used which is ABAQUS default amount. (4) K_C: is the rate of the second stress invariant in the tensile meridian to compressive meridian for any known value of the pressure invariant at initial yield. The value of Kc is in range (0.5-1) and its default value that used in ABAQUS is 0.667. (5) μ: represents the viscosity parameter which is used in ABAQUS to improve the convergence. Its default value is zero. The main CDP parameter values, especially dilation angle (ψ) and viscosity (μ), were implemented based on prior recommendations [39-41] and calibrated with the results of the study. Table 1 displays the assumed elastic and plastic properties for the designed concrete components in ABAQUS.

Table 1. The present numerical model's elastic and plasticity parameters

Parameters	Assumed Value
Elastic Parameters	
Elastic modulus E	36539
Poisson's ratio ν	0.2
Plastic Parameters	
K	0.667
Potential eccentricity ε	0.1
Dilation angle Ψ	51
fb_0/fc_0	1.16

CDP is utilized as a material model for normal concrete mixtures, due to its capacity to predict the reaction of all concrete structures and other quasi-brittle materials to static loads. CDP model assumes two mechanisms for failure which are: compressive crushing and tensile cracking. Also, this model takes in account the degradation in the material stiffness and the effect of stiffness recovery under cyclic loading. Based on CDP model, the concrete behaviors in compression and tension are identified through damage plasticity. The compressive behavior for concrete under uniaxial compressive load can be noticed in Figure 1(A), the stress-strain relationship in this figure can be divided into three stages: the first is linear-elastic relation up to yield stress (σ_o), in the second stage, stress hardening occurs until reaching the ultimate compressive stress value (σ_{cu}) followed by the last stage which is strain hardening. CDP model takes in account the degradation in the concrete stiffness at elastic through using the damage parameters dt (at tension) and dc (at compression) which are functions of strains in plastic stage and temperature. These variables change in limits (0 to 1) where zero mean un damaged material and 1 refers to completely lost for material strength. The flowing equations were used to calculate the damage parameters [41]:

$$d_t = 1 - \frac{\sigma_t}{\sigma_{tu}} \quad (1)$$

$$d_c = 1 - \frac{\sigma_c}{\sigma_{cu}} \quad (2)$$

Figure 1(A) demonstrates a standard stress-strain relation of uniaxial concrete compressive in the finite element model. This work provides stress-strain equations to characterize the compressive behavior of ordinary concrete seen in Figure 1(B), which are categorized into three stages: the elastic range, plastic behavior, and softening. The uniaxial stress-strain curve is changed into a stress-plastic strain representation in ABAQUS by adding stress and inelastic strain data. The computation of the inelastic strain, ε_c^{in} is as follows:

$$\varepsilon_c^{in} = \varepsilon_c - \varepsilon_c^{el} \quad (3)$$

where, $\varepsilon_c^{el} = \frac{\sigma_c}{E_0}$.

On the other hand, this study utilized tension damage measurements to assess the initiation of cracking in reinforced concrete slabs under different loads. However, they modeled the stress-strain curve of normal concrete in tension using a relation proposed by Massicotte et al. [42] as seen in Figure 2.

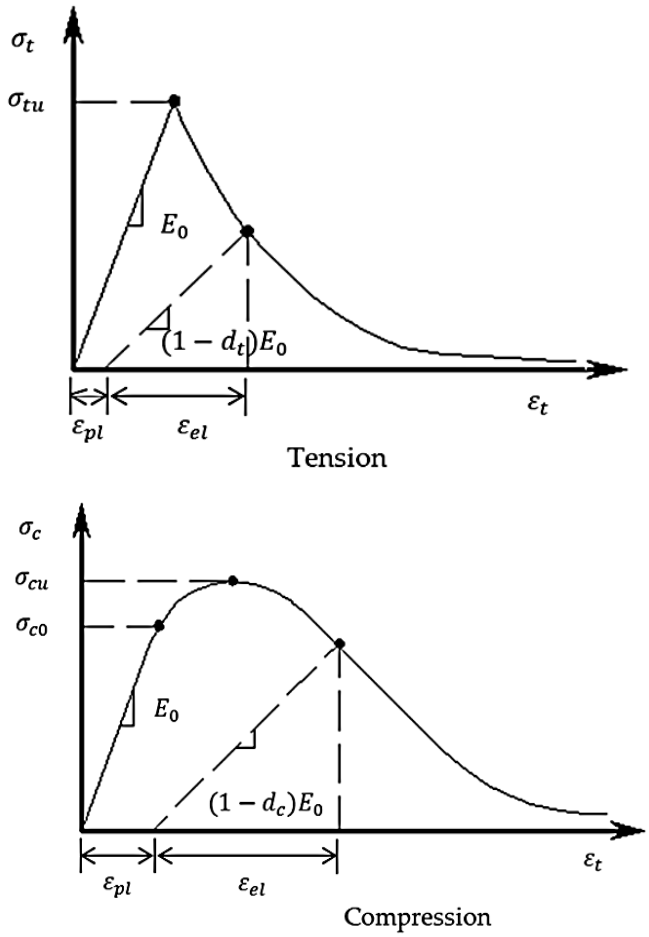

(A) Concrete response to uniaxial loading based on manual of the ABAQUS theory [43]

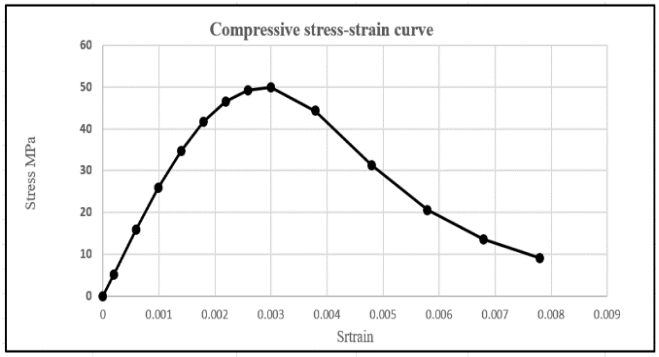

(B) Compressive stress strain curve

Figure 1. Stress-inelastic strain curve for normal concrete in compression [43]

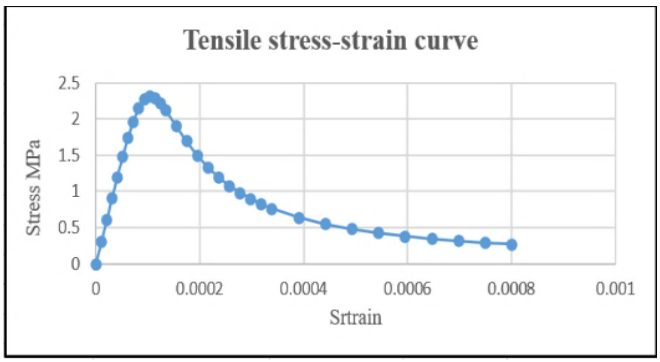

Figure 2. Tension softening curve for NC [43]

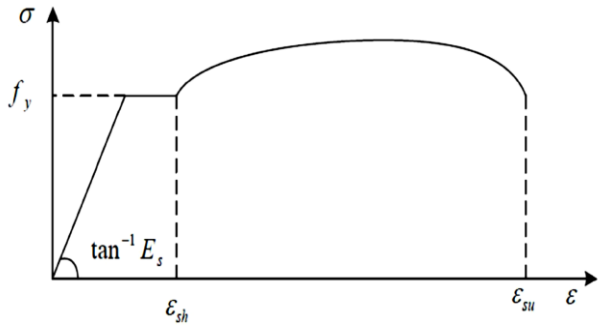

Figure 3. Curve of stress-strain for steel material [44]

Table 2. Characteristics of the steel bar

Bar Diameter, mm	Elastic Properties		Plastic Properties	
	Modulus of Elasticity (E)	Poisson's Ratio (υ)	Yield Stress (MPa)	Plastic Strain
Ø8	200000	0.3	298.39	0.006

For the reinforcement bars, Young's modulus E and Poisson's ratio υ, reflect the stress-strain relationship as shown in Figure 3. Where E is typically around 200,000 MPa and υ is around 0.3, Table 2 displays the plastic properties, such as the yield stress and the associated plastic strain.

Regarding the second component, the steel girder, steel is a homogenous material, exhibiting equal stress-strain behavior at specific levels of tension and compression. The computer models rely heavily on entering essential attributes to receive efficient and specific outcomes. Whole girder models were implemented with these properties, and the selected element requests the linear and nonlinear behavior properties. It may create an identical stress-strain relationship on both the tensile and compressive sides [44]. The relation with strain and stress may be separated into two components: the first has a slope of Es, while the second is expected to have a slope of zero; nevertheless, for computational analysis, it is represented with a slope of 0.01Es, as seen in Figure 4 [45]. Table 3 presents an overview of the characteristics utilized by ABAQUS in finite element analysis.

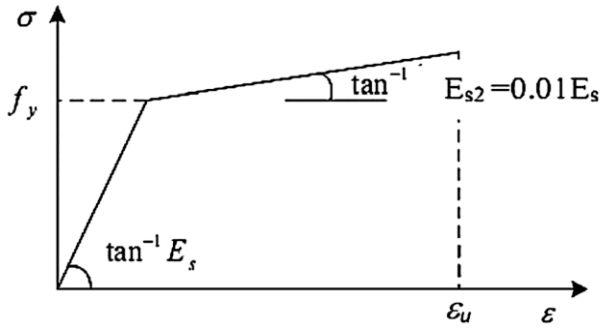

Figure 4. Curve stress-strain for steel material in ABAQUS [44]

Table 3. Characteristics of the steel girder

Elastic Properties		
Modulus of elasticity (E)		200000
Poisson's ratio (υ)		0.3
Plastic Properties		
Yield stress for flange (MPa)	f_y	225
	f_u	390
Yield stress for web and stiffener (MPa)	f_y	235
	f_u	400
Bolted shear connectors (M16)	f_y	932.43
	f_u	1040
Plastic strain for flange	ε_e	0
	ε_p	0.0825
Plastic strain for web and stiffener	ε_e	0
	ε_p	0.0825

2.2 Geometrical modelling

Solid elements in ABAQUS can experience both linear and complicated nonlinear analyses, incorporating contact, plasticity, and significant deformation [38, 46-48]. This work utilized structural analysis for the concrete slab, load-bearing plates, and end plates depicted in Figure 5, adopting the ABAQUS hourglass-controlled three-dimensional (3D) eight-node solid element (C3D8R) exhibiting reduced integration [49]. Further, a 2-node linear 3-D truss element known as T3D2 is available in ABAQUS [49, 50] and was utilized to model steel bars throughout the structural analysis. Nevertheless, as seen in Figure 6, shell components were used to illustrate structures characterized by one dimension where the thickness is considerably smaller than the other dimensions. The thickness is determined by the sectional property, which indicates each component independently in a three-dimensional shell plane corresponding to its dimensions. This model includes complete 3-D components, with element thickness defined by section properties, as detailed in Table 4. ABAQUS assigns only specific section characteristics utilizing this thickness. The thin steel panels are shown in Figure 7 [51], which is a three-dimensional model made up of rectangular S4R shell elements or triangle elements, each with

six degrees of freedom at each node.

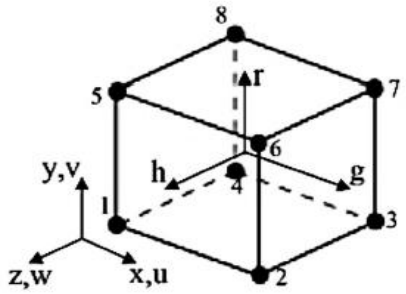

Figure 5. (C3D8) in ABAQUS [46]

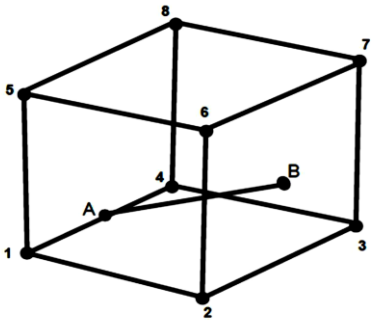

Figure 6. 2-Node 3-dimension truss element [46]

Table 4. Thickness and type element

Element	Thickness, mm	Element Type
Flange	5	Shell: planar
Flat web	3	Shell: planar
Stiffener	6	Shell: planar

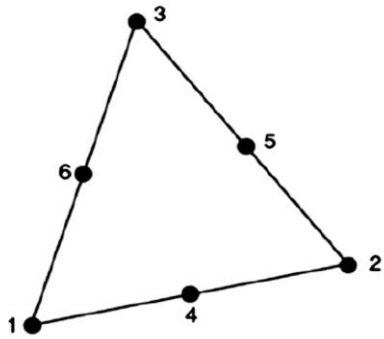

(a) Triangular elements

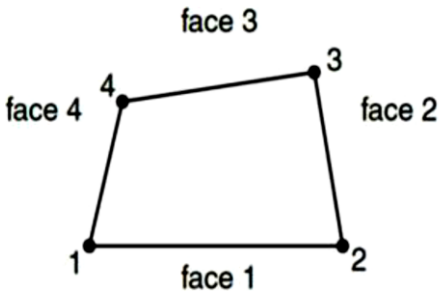

(b) Rectangular elements

Figure 7. Node shell element [51]

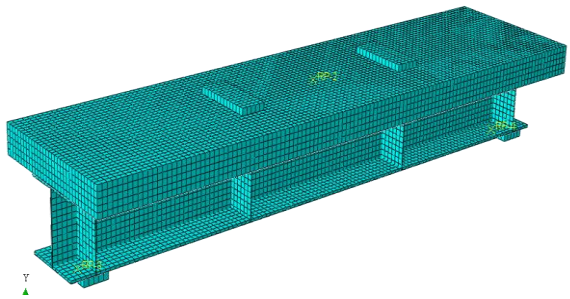

(a) Composite beam model in ABAQUS

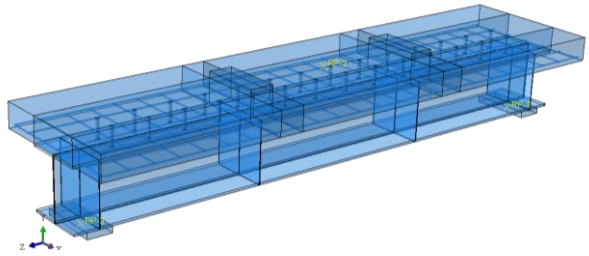

(b) Steel and studs reinforcement

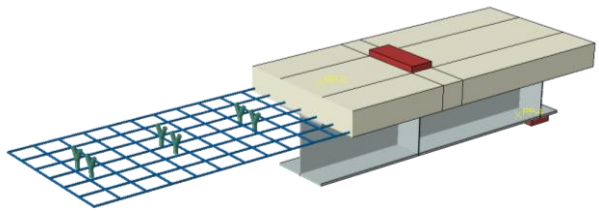

(c) Y-rib reinforcement

Figure 8. Assemblage of the RC column numerical models

2.3 Assembly of the numerical model

Figure 8 illustrates the assembly of every component included in the numerical model for this study. Stress localization in the loading and supporting areas has been minimized through the use of steel plates measuring 600 × 150 × 10 mm. The connected form of the CONSTRAIN option in ABAQUS was employed for attaching these plates to the composite beams. The simply supported boundary conditions that were employed in the experimental test were simulated by modeling the boundary conditions of the beams. Pin support: The node is fixed along the transverse line to the lower middle of the support plate, resisting translation in all directions vertical (direction Y), lateral (direction x), and longitudinal (z-direction). The contract is free to rotate around all the axes. Roller support: The nodes are fixed along the transverse line at the middle bottom of the support plate, translating only in one vertical direction (y direction). The contract is free to rotate around all axes.

Figures 5 and 6 present the loading and boundary conditions of the finite element model. Additionally, truss elements were employed in this study to represent the reinforcing bars, which were confined inside concrete solid components ("host" continuum) by the application of embedded region constraints in ABAQUS. Furthermore, the web was interconnected with the upper and lower flanges and stiffeners, and sections of the web were joined using tie contact, employing master and slave to set up the interaction as seen in Figures 5 and 6. Figure 8 illustrates the interaction of the steel girder, steel reinforcement, and concrete.

2.4 Meshing

To obtain reliable results for the finite element model, each component is carefully adjusted to correspond with the specific mesh size, offering that all disparate materials connect at the same node. The preferred mesh form in the model is a hexahedral (brick) structural element. Eight-node brick components with three degrees of freedom (C3D8) per node are employed to simulate the concrete and supporting plates of the mesh. A certain steel bar is designated as a T3D2 truss element. The mesh size of 20 mm gives the most accurate results depends on the aggregate size according to ABAQUS guideline 6.14. Therefore, 20 mm mesh size was adopted here for all specimens.

3. NUMERICAL TEST

This research is defined by a numerical investigation that compares the test results of previous experimental work by Li et al. [52] with the finite element analysis results of the present study. Li et al. [52] cast and tested twelve reinforced concrete composite beams under static loads until they failed. For this study, all the composite beams were made using the Chinese Code GB50017-2017 for building with steel and the Chinese Code GB50010-2010 for building with concrete. The tested composite beams were made from a hot-rolled steel section from China that is HM250 × 125 × 6 × 9 mm. All tested composite beam specimens had concrete slabs with a thickness of 100 mm, a width of 600 mm, and a length of 2350 mm (as seen in Figure 4). Six specimens were made with rectangular web openings measuring 300 mm in width and 150 mm in depth. The dimensions of the web hole are mainly determined to permit the passage of various pipes, including those for water, power, heating, and communication. The high-strength bolts that were used were all grade 10.9, M16 × 120 mm hexagonal high-tension friction-grip bolts. The bolt holes of the composite beam samples were drilled. Figure 4 presents more details about the schematic shape, while Table 5 provides the configurations of the composite beam specimens. For the concrete utilized in the concrete slab specimens, the average compressive strength (fc') values are 30 MPa. Figure 9 presents the longitudinal view for tested composite beams. On the other hand, Table 6 identifies the parameters of the tested beams. Using a universal testing instrument, all reinforced concrete beams were subjected to a static load until they failed as shown Figure 10. The test was conducted using a 50T pressure testing device under a monotonic focused load. The standard test techniques specified in the Standard for Test Method of Concrete Structures (Chinese Code GB/T50152-2012) were utilized. The specimen was subjected to two cycles of loading and unloading to prevent relaxation in the loading device components and then reloading until the specimen was destroyed.

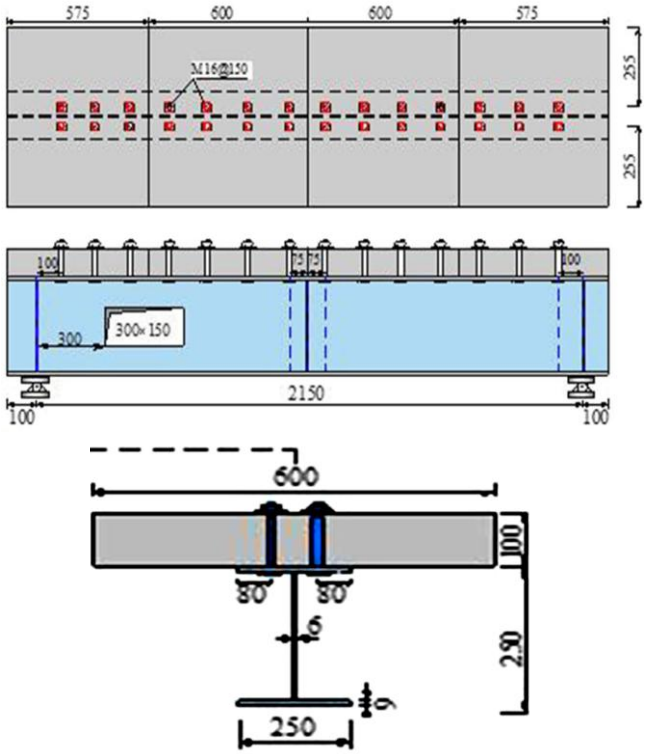

Figure 9. Details of the adopted beam elements [52]

Figure 10. Test rig used in this study [52]

Table 5. Details of the tested beams

Beam Designation	Connection Ratio	Number of Openings	Shape of Openings	Location of Openings	Type of Connector	Stud Spacing
C50S	50%	0	…….	……	Stud	7@342
C70S	70%	0	……	……	Stud	10@222
C100S	100%	0	…..	……	Stud	14@150
C50RS	50%	1	Rectangular	Center	Stud	7@342
C70RS	75%	1	Rectangular	Center	Stud	10@222
C100RS	100%	1	Rectangular	Center	Stud	14@150
C50Y	50%	0	……	……	Y-Rib	7@342
C75Y	75%	0	…….	……	Y-Rib	10@222
C100Y	100%	0	……	……	Y-Rib	14@150
C50RY	50%	1	Rectangular	Center	Y-Rib	7@342
C70RY	75%	1	Rectangular	Center	Y-Rib	10@222
C100RY	100%	1	Rectangular	Center	Y-Rib	14@150

Table 6. Notation of the tested beams

Beam Designation	Beam Details
C-50S	Composite beam-50% connections ratio- stud connections
C-70S	Composite beam-70% connections ratio- stud connections
C-100S	Composite beam-100% connections ratio- stud connections
C-50RS	Composite beam-50% connections ratio- rectangular web opening- stud connections
C-70RS	Composite beam-70% connections ratio- rectangular web opening- stud connections
C-100RS	Composite beam-100% connections ratio- rectangular web opening- stud connections
C-50Y	Composite beam-50% connections ratio- Y-rib connections
C-70Y	Composite beam-70% connections ratio- Y-rib connections
C-100Y	Composite beam-100% connections ratio- Y-rib connections
C-50RY	Composite beam-50% connections ratio- rectangular web opening- Y-rib connections
C-70RY	Composite beam-70% connections ratio- rectangular web opening- Y-rib connections
C-100RY	Composite beam-100% connections ratio- rectangular web opening- Y-rib connections

4. NUMERICAL RESULTS AND DISCUSSIONS

Twelve composite beams made with normal concrete were prepared to investigate their structural behavior. Six specimens, which were made of bolt connections, were tested until failure, while the others were made from Y-rib connections. On the other hand, six beams are made with rectangular web openings with dimensions 300x150mm. Table 7 and Figures 11 and 12 summarise the numerical test results for the beam specimens, including their ultimate capacity, failure load, and failure mode. The subsequent parts analyze and assess the results of the load-displacement curves.

Table 7. Numerical results for the tested composite beams

Beam Designation	Connection Ratio (%)	Type of Connector	Ultimate Capacity (kN)	Failure Load Increase Over Control Beam*(%)	Δ_{max} (mm)	Ratio Relative to the Control Beam*	Failure Mode
C-50S	50	Stud	1083.14	--	24.47	--	Shear Failure
C-70S	70	Stud	1100.94	+1.64	25.74	+5.19	Shear Failure
C-100S	100	Stud	1107.96	+2.29	31.65	+29.34	Shear Failure
C-50RS	50	Stud	1113.27	--	44.06	--	Shear Failure
C-70RS	70	Stud	1120.69	+0.67	33.05	-24.99	Shear Failure
C-100RS	100	Stud	1145.98	+2.94	36.78	-16.52	Shear Failure
C-50Y	50	Y-rib	1103.45	--	50	--	Shear Failure
C-70Y	70	Y-rib	1125.99	+2.04	50	0.00	Shear Failure
C-100Y	100	Y-rib	1143.58	+3.64	50	0.00	Shear Failure
C-50RY	50	Y-rib	1102.37	--	50	--	Shear Failure
C-70RY	70	Y-rib	1123.94	+1.96	50	0.0	Shear Failure
C-100RY	100	Y-rib	1138.93	+3.32	50	0.0	Shear Failure

*This is the ratio of the ultimate load of beams relative to the control beam with 50% connection ratio (studs and Y-rib connections), (+) means increase (%) in the above properties with respect to reference beam, (-) means decrease (%) in the above properties.

4.1 Effect of shear connections ratio

(1) Load-mid span deflection response

In this group, six composite beams were previously mentioned, which were produced with different shear connections (bolt studs and Y-rib connection). Three specimens made with bolt studs have various connection ratios (50%, 70%, and 100%). However, the other tested beams featured Y-rib connections with percentages of 50%, 70%, and 100%. When comparing the numerical results of this group of composite specimens [C-50S, C-70S, and C-100S], which were tested under static loading, it can be noted that shear failure occurred for these tested specimens. Table 8 and Figure 13 present the numerical outcomes of the tested beam specimens. Figure 13 demonstrates that all tested beams maintain their linear behaviour up to the first crack. Thereafter, the load-deflection curve becomes nonlinear, leading to a decrease in the specimen's stiffness when the diagonal shear cracking starts to develop and increases until the beam fails. The results indicated that the initial stiffness (service-region slope) increases when the shear-connection ratio (SCR) is raised in the composite section. Increasing the connections ratio from 50% to 70% typically produces a significant increase in stiffness; however, going from 70% to 100% provides additional stiffness but with diminishing returns as the section approaches full composite action. Therefore, the load–deflection curve becomes steeper (less deflection under the same load) as SCR increases. When comparing the load-displacement curves of bolt studs beams C-50S, C-70S, and C-100S with different connection ratios, the maximum load-carrying capacity was 1083.14 kN, 1100.94 kN, and 1107.96 kN, respectively. In addition, the mid-span displacements for tested beams were 24.47 mm, 25.74 mm, and 31.65 mm, respectively. From Table 7, the tested result presents that the increased connections ratio enhanced the ultimate failure load by approximately 1.64% and 2.29% compared to control beams. Conversely, compared to reference beams, the deflection value increased by approximately 5.19% and 29.34%. Figure 13 reveals that the tested C-100S beam had a higher stiffness than the other tested beams (C-50S and C-70S beams). As a result, the ultimate strength of tested specimens reduced when bolt spacing increased, namely at spacings of 150 mm, 222 mm, and 342 mm. Thus, higher SCR shifts the structure towards flexural capacity controlled by the composite section (higher moment capacity). Further, at low SCR (≈50%) the beam may show earlier relative slip, interface debonding, and a lower ultimate moment—failure may be governed by connector failure or local concrete crushing rather

than full-section flexural yielding. However, near 100% SCR, the ultimate load is higher, and failure tends to be governed by steel flange yielding or concrete compression block failure.

Regarding the beams made with Y-rib connections with 50%, 70%, and 100% connection ratios, it was obviously observed that these C-100Y beams exhibited higher stiffness than those of tested beams (C-50Y and C70Y beams). The increase was 2.04% and 3.64% for C-70Y and C-100Y; see Table 7. It was apparent from Figure 14 that the Y-rib composite beam specimen failed in shear failure mode and seemed more ductile compared to other tested beams. Y-ribs create a continuous or semi-continuous shear transfer path, reducing local stress concentrations and corner/high-gradient shear zones. Fewer local peaks mean less local cracking/punching in the concrete and a lower tendency for connector pull-out. Thus, wider contact reduces bearing stress on the concrete, delaying local crushing and improving load capacity. This means that ribs engage the concrete slab more uniformly, restraining relative rotation and vertical uplift that produce slip. Further, the effective lever arm for shear transfer is often larger because Y-ribs engage a larger area with the enhanced composite lever arm—improving overall moment capacity. On the other hand, better performance near discontinuities (openings): around web openings (rectangular or circular), the web and flange stresses redistribute; Y-ribs better bridge disturbed shear paths and are less sensitive to local geometry (corner effects) than studs. From Figure 11, studs exhibit discrete load–slip curves (initial stiffness, possible plateau, and ultimate shear failure). Y-ribs show a smoother, stiffer load–slip response because load is carried by larger area and multiple micro-paths. the Implications for design and construction was that using higher SCR (near 100%) when the priority is maximum stiffness, minimal deflection, and full utilization of composite capacity (long spans, serviceability-sensitive floors, and heavy live loads). Thus, consider partial connection (≈70%) where some economy is required and some added ductility is desired—often gives most of the stiffness with fewer connectors (good cost-benefit). 50% or lower is acceptable in lightly loaded or intentionally partially composite designs but must be justified with serviceability checks and slip limits. On the other hand, Y-rib connections are preferred for prefabricated/industrial construction where ribs can be fabricated into sections offsite and cast integrally with precast slabs.

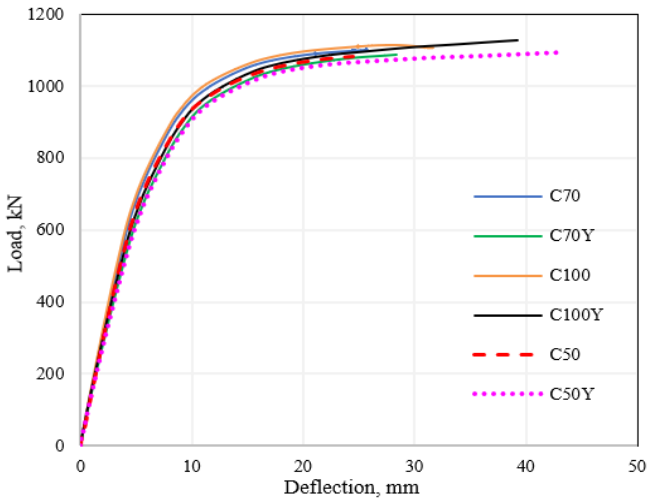

Figure 11. Load–deflection response for composite beams with different shear connector

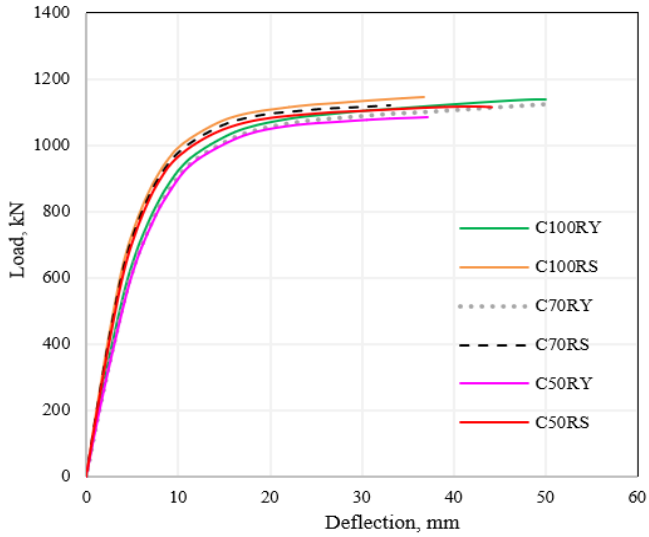

Figure 12. Load–deflection response for opening web composite beams with different shear connector

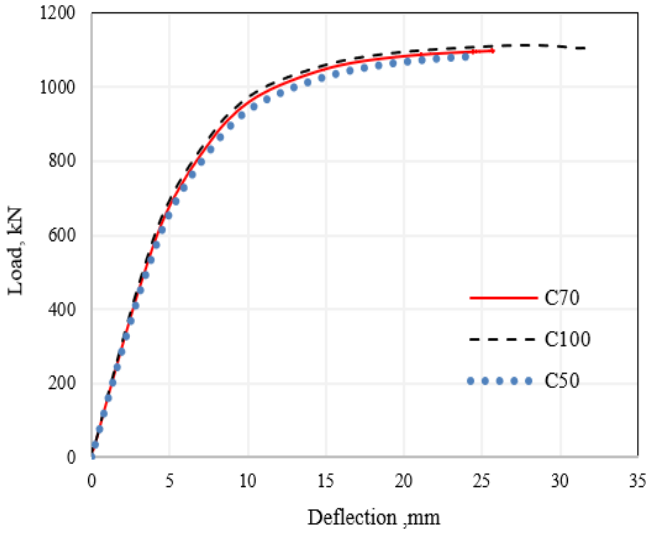

Figure 13. Load–deflection response for composite beams with bolt studs connections

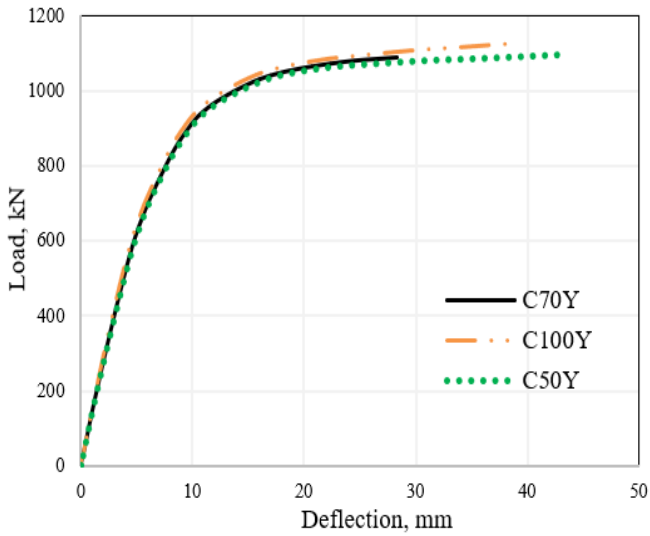

Figure 14. Load–deflection response for composite beams with Y-rib connections

Table 8. The ultimate loads and deflection of the tested beams with different shear connections ratio

Beam Designation	Connection Ratio (%)	Type of Connector	Ultimate Capacity (kN)	Failure Load Increase Over Control Beam* (%)	Δ_{max} (mm)	Ratio Relative to the Control Beam*	Failure Mode
C-50S	50	Stud	1083.14	--	24.47	--	Shear Failure
C-70S	70	Stud	1100.94	+1.64	25.74	+5.19	Shear Failure
C-100S	100	Stud	1107.96	+2.29	31.65	+29.34	Shear Failure
C-50Y	50	Y-rib	1103.45	--	50	--	Shear Failure
C-70Y	70	Y-rib	1125.99	+2.04	50	0.00	Shear Failure
C-100Y	100	Y-rib	1143.58	+3.64	50	0.00	Shear Failure

*This is the ratio of the ultimate load of beams relative to the control beam with 50% connection ratio, (+) means increase (%) in the above properties with respect to reference beam, (-) means decrease (%) in the above properties.

(2) Crack patterns and failure modes

Figures 15 and 16 illustrate the failure mode of all tested beams with different types of shear connectors (C-100S, C-70S, C-50S, C-100Y, C-70Y, and C-50Y beams). It can be observed that all the tested composite beams showed shear failure modes. For all tested beams with studs and Y-rib connections, various connection ratios were 50%, 70%, and 100%. The crack patterns observed in the composite beams demonstrated a clear relationship with both the type of shear connection and the shear connection ratio (Figure 15). In beams strengthened with shear studs, initial cracks generally formed in the concrete slab close to the steel–concrete interface, particularly near the connectors. These early cracks were typically inclined or vertical, corresponding to high principal tensile stress regions and concentrated shear transfer zones predicted by the numerical simulations. Localized radial cracks and small crushing areas beneath stud heads were also evident, a result of concentrated bearing stresses. As the load increased, these cracks propagated and interconnected, causing progressive slip along the interface and a gradual reduction in stiffness. This behavior was most pronounced at lower shear connection ratios, where the reduced number of connectors allowed greater relative movement between the steel beam and concrete slab, accelerating the deterioration of composite action.

In beams fitted with Y-rib connectors (Figure 16), the cracking behavior differed significantly. Instead of a few dominant cracks developing early, a fine network of distributed microcracks formed progressively, and major splitting cracks were delayed until much higher load levels. The broader contact area and continuous shear transfer path of the Y-rib reduced peak tensile and bearing stresses in the concrete and promoted a more uniform distribution of shear flow along the interface. This reduced the severity of local damage and delayed the onset of significant slip, particularly at higher connection ratios, where composite action was sustained almost to ultimate load. The influence of shear connection ratio was evident in the load–deflection and crack development behavior. At a 50% connection ratio, initial stiffness was noticeably lower; cracks formed earlier, and deflections increased rapidly after the onset of interface slip. The reduced connector density meant that individual connectors were more heavily loaded, intensifying local stresses and leading to earlier crack coalescence and partial loss of composite action. At a 70% connection ratio, stiffness improved substantially, cracking was delayed, and the growth rate of deflection was reduced, representing a balance between material economy and structural performance. At full connection, stiffness and ultimate load capacity were maximized, cracking in both stud- and Y-rib-strengthened beams was significantly reduced, and failure typically occurred through yielding of the steel or crushing of the concrete in the compression zone rather than by interface degradation.

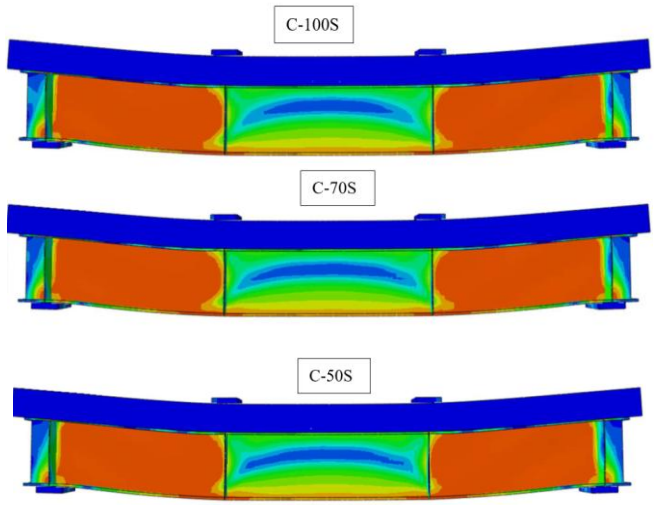

Figure 15. Crack patterns and mode of failure for the tested beams (Beams with studs connections)

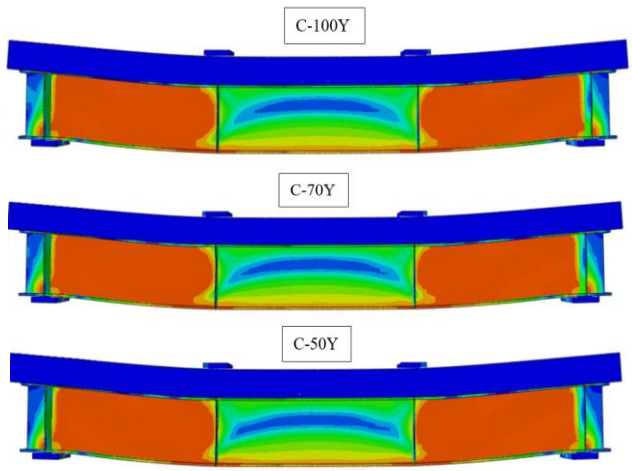

Figure 16. Crack patterns and mode of failure for the tested beams (Beams with Y-rib connections)

The previous experimental result testing observations align closely with the numerical predictions, which showed higher stress concentrations and earlier slip at low connection ratios and more uniform stress distribution with delayed cracking at higher connection ratios. These trends are also consistent with existing literature, which emphasizes that increasing the degree of shear connection enhances composite stiffness, delays crack initiation, and shifts the governing failure mode from brittle interface failure to more ductile flexural failure.

The superior performance of Y-rib connectors across all connection ratios further confirms their advantage in reducing local stress peaks, distributing shear more evenly, and maintaining composite action under higher loads.

4.2 Effect of type shear connections

(1) Load-mid span deflection response

A comparison of load-displacement curves is illustrated in Figures 17-19 for six composite beams reinforced with similar shear connection spacing (50%, 70%, and 100% connection ratio), but with different types of connections, which were bolt studs and Y-rib sorts. Three groups include two beams designated with the same connection ratio and different types of shear connections (bolts and Y-rib types), as shown in Table 9. The load–deflection response of composite beams showed a clear dependency on the type of shear connection used. Beams strengthened with conventional shear studs exhibited a gradual increase in load capacity with deflection, followed by a more pronounced curvature in the load–deflection curve as slip at the steel–concrete interface began to develop. In contrast, beams strengthened with Y-rib connections demonstrated a stiffer initial response, higher peak load capacity, and reduced mid-span deflections at comparable load levels, as shown in Figures 17-19. Comparing the load-displacement curves of all tested beams C-50S, C-70S, C-100S, C-50Y, C-70Y, and C-100Y, the maximum load-carrying capacity of these tested beams was 1083.14 kN, 1100.94 kN, 1107.96 kN, 1103.45 kN, 1125.99 kN, and 1143.58 kN, respectively; see Table 7. As a result, Y-rib connection beams present an increase of approximately 1.88%, 2.28%, and 3.215%, respectively, when compared to bolt stud beams. Conversely, the mid-span deflection of the Y-rib tested beams has increased by approximately 104.33%, 94.25%, and 57.98% in comparison to the reference beams. This enhanced performance of the Y-rib system can be attributed to its larger bearing area, improved mechanical interlock, and ability to engage more of the concrete slab in load transfer, thereby minimizing localized slip and better maintaining composite action throughout loading. The Y-rib shear connector demonstrated the most advantageous results due to its strong bonding within the mass of concrete on both ends.

Mechanically, the superior performance of the Y-rib is explained by its geometry, which provides both vertical and inclined bearing surfaces that resist relative displacement between the slab and the steel flange. This arrangement increases the load transfer efficiency, reducing interface slip and ensuring that the concrete slab participates more effectively in resisting bending moments. Reduced slip also limits the redistribution of stresses that typically leads to early stiffness degradation in shear stud-only connections. As a result, the Y-rib system sustains higher stiffness over a greater portion of the load range and delays the onset of inelastic deformations in both the steel and concrete components. From a design and construction perspective, these findings have significant implications. For structures where serviceability limits—such as deflection control—are critical, Y-rib connections can provide superior performance without requiring an increase in the number of connectors. In addition, by reducing slip and improving stiffness, Y-ribs may allow for smaller slab thicknesses or lighter steel sections without compromising strength or serviceability. However, the fabrication complexity and potential welding requirements of Y-ribs must be weighed against these benefits during design and detailing. In critical applications such as long-span floors or bridges, the enhanced stiffness and reduced deflection of Y-rib systems offer a clear advantage, potentially extending service life and reducing maintenance needs.

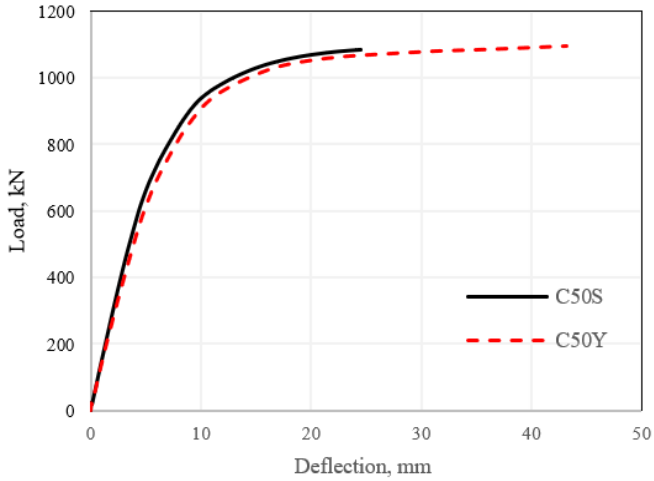

Figure 17. Load–deflection response for composite beams reinforced with 50% spacing of shear connection

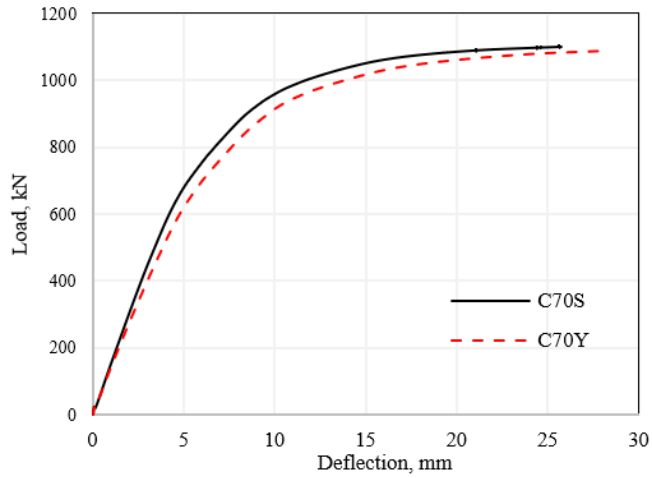

Figure 18. Load–deflection response for composite beams reinforced with 70% spacing of shear connection

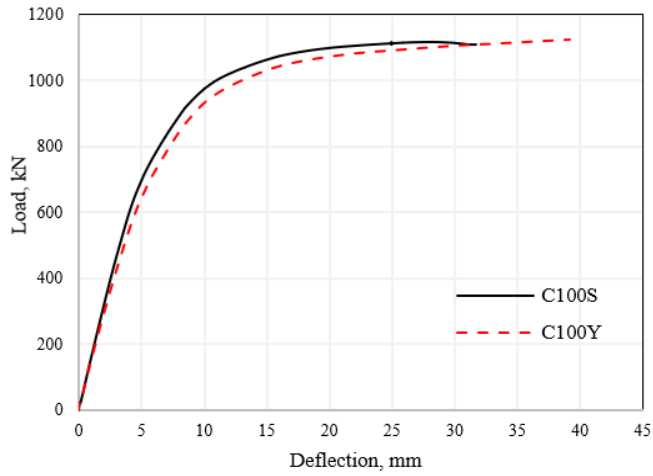

Figure 19. Load–deflection response for composite beams reinforced with 100% spacing of shear connection

Table 9. The ultimate loads and deflection of the tested composite beams with different type of shear connections

Beam Designation	Connection Ratio (%)	Type of Connector	Ultimate Capacity (kN)	Failure Load Increase Over Control Beam* (%)	Δ_{max} (mm)	Ratio Relative to the Control Beam*	Failure Mode
C-50S	50	Stud	1083.14	--	24.47	--	Shear Failure
C-50Y	50	Y-rib	1103.45	+1.88%	50	+104.33%	Shear Failure
C-70S	70	Stud	1100.94	--	25.74	--	Shear Failure
C-70Y	70	Y-rib	1125.99	+2.28%	50	+94.25%	Shear Failure
C-100S	100	Stud	1107.96	--	31.65	--	Shear Failure
C-100Y	100	Y-rib	1143.58	+3.21%	50	+57.98%	Shear Failure

*This is the ratio of the ultimate load of beams relative to the control beam with bolt studs connections, (+) means increase (%) in the above properties with respect to reference beam, (-) means decrease (%) in the above properties.

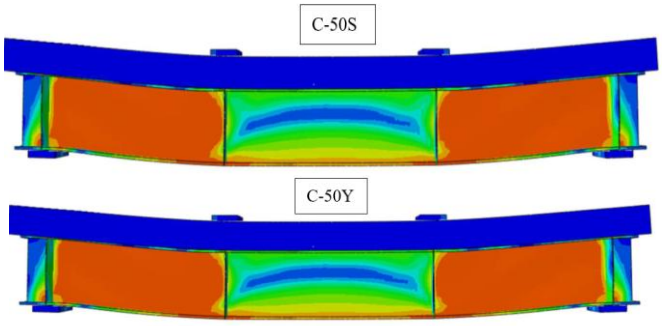

Figure 20. Crack pattern and failure mode for composite beams reinforced with 50% spacing of shear connection

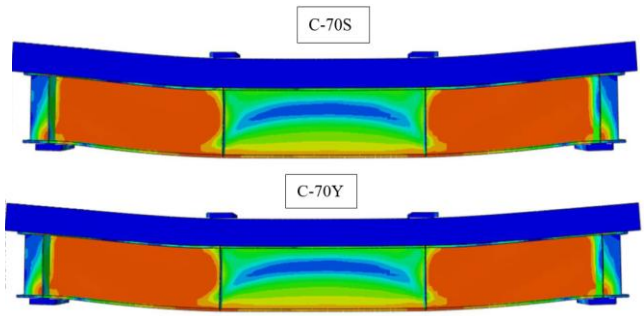

Figure 21. Crack pattern and failure mode for composite beams reinforced with 70% spacing of shear connection

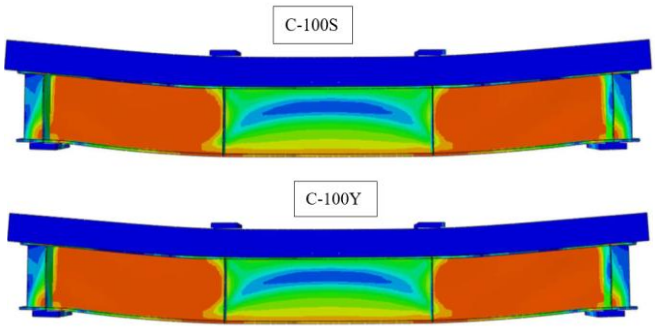

Figure 22. Crack pattern and failure mode for composite beams reinforced with 100% spacing of shear connection

(2) Crack patterns and failure modes

Shear connectors are essential for the efficacy of composite tested beams; they primarily support the transfer of shear stresses which enhance composite action in the concrete element and the steel beam, thereby improving load-carrying capacity, crack distribution, and overall efficiency of the composite beam. Figures 20-22 show the crack patterns and failure modes of the bolts and Y-rib connection composite beams with various connection ratios. In the specimens with shear stud connections, the finite element (FE) models indicated high interfacial shear stresses concentrated near the connectors, especially in the regions adjacent to the steel top flange. These local stress peaks corresponded to the earliest observed cracks in the experimental program—fine flexural cracks in the slab's tension zone directly above and between the studs. As the load increased, these cracks extended vertically toward the compression zone, and secondary diagonal cracks formed in the shear span, consistent with the regions of high principal tensile stress predicted numerically. Near failure, the localized slip between steel and concrete, also indicated by increased connector shear demand in the FE results, contributed to a mixed flexural–shear failure mode with concrete crushing at mid-span and yielding of the steel section. The results demonstrate the impact of various shear connector types in comparison to the typical connector (Bolt studs' connections), this illustrates the enhancement in total load capacity and deflection but a similar behavior in crack morphology and failure mode compared to the conventional method by using stud shear connectors.

In the Y-rib connection specimens, the simulations showed a more uniform stress transfer across the steel–concrete interface and lower peak shear stresses around the connectors (Figures 20-22). Experimentally, this manifested as a delayed onset of shear cracks, smaller crack widths, and a more evenly distributed crack pattern along the slab. Diagonal cracking in the shear span appeared at higher load levels than in the stud-connected beams, reflecting the improved shear transfer efficiency and reduced slip at the interface predicted by the FE models. Failure in Y-rib beams was dominated by concrete crushing in the compression zone and yielding of the steel section, with minimal interface separation—indicating a predominantly ductile flexural failure mode. In addition, the results indicated that the Y-rib shear connection exhibits superior resistance compared to the typical stud shear connector, as well as enhanced deflection characteristics. This results from conforming to the same mechanics used in the conventional method, which accounts for the similarity in failure patterns by causing the concrete and steel components to separate through slippage.

The alignment between the numerical and experimental findings supports the accuracy of the FE stress predictions in identifying critical crack initiation zones. The transition from early localized cracking and mixed-mode failure in shear stud beams to delayed cracking and more ductile flexural failure in Y-rib beams is consistent with previous research on composite beams, which emphasized that enhanced interlock connections reduce interface slip, improve stress distribution, and shift the failure mechanism toward a more favorable ductile response.

4.3 Effect of rectangular web opening

(1) Load-mid span deflection response

A rectangular web opening for tested composite beams made with different types of shear connectors (Bolts studs and Y-rib connections) was used to investigate the shear load-deflection responses of the beams, which are depicted in Table 10 and Figure 23. Three connection ratios, 50%, 70%, and 100%, were used for each type of connection. For bolt stud connections, three web-opening specimens designated as C-50RS, C-70RS, and C-100RS exhibited a quasilinear response until the peak load. Under service loading, specimens strengthened only with discrete shear studs typically show reduced initial stiffness and larger mid-span deflections compared with intact webs, because the opening forces the longitudinal shear flow to detour around the hole and concentrates shear and tensile stresses near the opening edges. The opening specimens show a slight increase in the maximum failure loads of 2.78%, 1.79%, and 3.43% for C-50RS, C-70RS, and C-100RS, respectively, compared to beams without openings. However, an increase in deflection response of approximately 80.06%, 28.40%, and 16.22%, respectively, when compared to non-opening specimens, is presented in Table 9. Figure 24 shows the shear load-deflection response of the opening beams with bolt stud connections. The present web opening for composite beams improved the shear response of the non-opening beams. These local stress concentrations—especially at the sharp corners of a rectangular opening—promote earlier crack initiation in the slab and localized concrete damage adjacent to the flange, which in turn permits relative slip between the steel and concrete to develop sooner. These specimens did not demonstrate a reduction in load or a notable variation in slope at the initiation of shear cracking.

In contrast, opening Y-rib beams reduces the maximum shear strength by about 0.1%, 0.18%, and 0.41% for C-50RY, C-70RY, and C-100RY, respectively, compared to beams without openings. The results also indicated that there were no changes in deflection values at failure loads. When the same geometry is strengthened with Y-rib (perfobond-type) connections, the global load–deflection behaviour is usually stiffer and the mid-span deflections at equivalent load levels are smaller. The Y-rib's continuous or semi-continuous interface contact provides a broader bearing area and multiple load paths across the disturbed region, allowing shear to be distributed over a larger area instead of being concentrated at discrete points. This more uniform shear transfer reduces the peak tensile and bearing stresses predicted by finite-element models around the opening perimeter, delays crack initiation, and therefore postpones the onset of significant connector slip. Furthermore, the results indicated that there were no corresponding changes in deflection values at failure loads. Additionally, as shown in Figure 24, the stiffness of opening beams is similar to that of reference beams (beams without openings). Consequently, load–deflection curves for Y-rib-strengthened beams exhibit a steeper initial slope, a longer elastic range, and a higher ultimate load before either steel yielding or concrete compression governs failure.

Mechanically, the superiority of the Y-rib in the presence of a rectangular opening can be explained by three interacting effects. First, the larger contact and bearing area of the rib reduces local bearing pressure and the risk of radial cracking or local concrete crushing beneath connectors. Second, the rib creates a bridging action across the disturbed shear path, effectively reintroducing continuity in shear transfer around the cutout; this reduces shear-flow rerouting and the associated tensile peaks at corners that drive splitting cracks. Third, Y-ribs provide enhanced restraint against slab uplift and relative rotation of the flange and slab, which limits the relative movements that manifest as interface slip and amplified deflections. These mechanics combine to produce a collective connector response that is stiffer and more ductile than that of isolated studs, particularly when openings interrupt the typical distribution of shear flow.

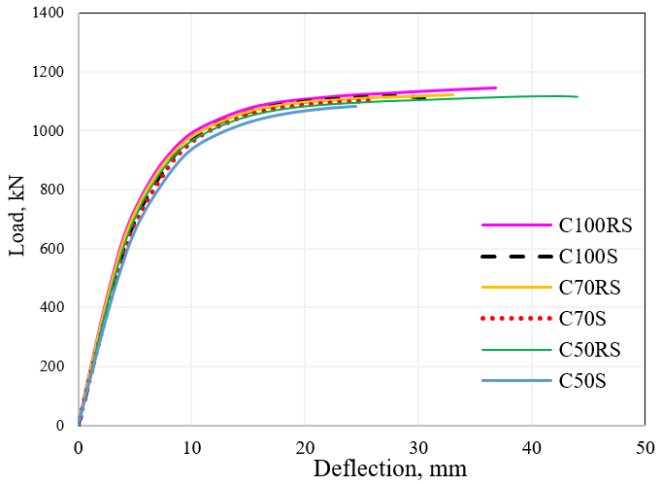

Figure 23. Load–deflection response for the tested composite beams made with and without rectangular web opening reinforced bolts shear connections

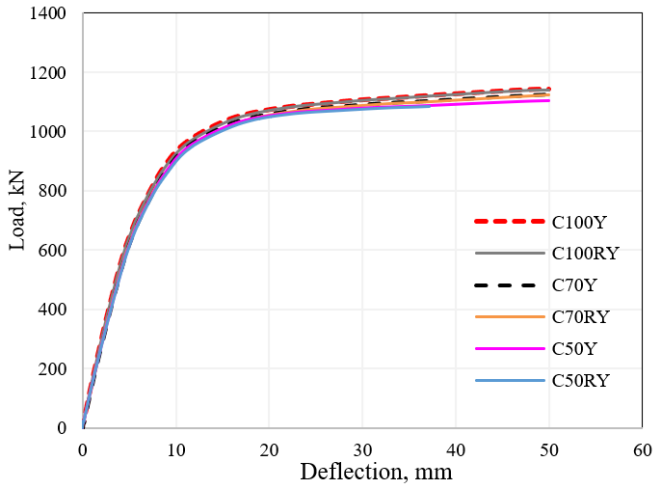

Figure 24. Load–deflection response for the tested composite beams made with and without rectangular web opening reinforced Y-rib shear connections

(2) Crack patterns and failure modes

Figures 25 and 26 present the crack patterns and failure mode for tested opening composite beams. For all tested opening beams, diagonal cracks initially appeared in the edges of the web openings and extended to the concrete block surrounding the loading site when the load approached approximately 50% of the ultimate load. When the load on samples heightened, the impact of additional bending moments due to "Vierendeel action" adjacent areas of a web opening, along with the extrusion impacts between proximate concrete panels, became increasingly evident. Shear failure in tested specimens was exhibited suddenly upon application of

the ultimate failure load. Cracks consistently initiated at locations of highest predicted tensile demand: fine flexural cracks first developed in the slab tension zone where the FE principal tensile contours peaked under midspan bending (see Figure 25), while a second family of cracks formed along the disturbed shear path adjacent to the opening where the simulations showed concentrated shear flow and elevated interface tensile stresses (see Figure 25). In specimens with discrete studs, the models predicted sharp local peaks of bearing and shear stress beneath stud heads and high interfacial shear gradients between studs; experimentally this was manifested as short radial cracks and local crushing under studs, together with inclined cracks emerging above and between studs. As loading progressed these local cracks followed the principal stress trajectories in the FE maps, coalescing into continuous crack lines that coincided with the numerical zones of connector overload and sharply rising slip. The numerical load-slip response captured the corresponding stiffness degradation: as connector demand exceeded local capacity the model showed reduced tangent stiffness and increased relative displacement, mirroring the experimentally observed softening in the load–deflection curves.

Beams strengthened with continuous Y-rib connectors exhibited a markedly different stress state in the simulations and a correspondingly different crack morphology in the tests. The FE results for Y-ribs showed a broader, smoother shear-transfer field and substantially lower peak bearing and tensile stresses at any single contact point. Experimentally this produced a dense network of fine, distributed microcracks rather than a few large localized splits; the interface retained compatibility to higher loads and major splitting was delayed. In effect, the Y-rib redistributed shear around the disturbed region, reduced local stress concentrations that drive crack initiation, and preserved composite action until global flexural mechanisms-controlled failure. The final collapse in ribbed specimens therefore matched the simulations' prediction of ductile flexural failure (steel yielding or compression-zone crushing) rather than brittle connector or local concrete failure. For design and testing this linkage has three immediate implications. First, FE principal tensile stress plots should be used to guide local reinforcement or stiffener placement and to determine safe connector spacing so as to avoid predicted tensile peaks. Second, when simulations indicate concentrated bearing or shear peaks, designers should either change the connector system to a distributed form (e.g., Y-ribs) or provide local concrete/steel reinforcement to mitigate splitting and crushing. Third, in validating models against experiments, crack initiation location and timing are more discriminating metrics than global load capacity alone; matching these local indicators increases confidence that the model will predict failure mode correctly for alternate geometries and load cases.

Table 10. The ultimate loads and deflection of the tested rectangular web opening composite beams made with bolts and Y-rib shear connections

Beam Designation	Connection Ratio%	Type of Connector	Ultimate Capacity (kN)	Failure Load Increase Over Control Beam* (%)	Δ_{max} (mm)	Ratio Relative to the Control Beam*	Failure Mode
C-50S	50	Stud	1083.14	--	24.47	--	Shear Failure
C-50RS	50	Stud	1113.27	+2.78%	44.06	+80.06%	Shear Failure
C-70S	70	Stud	1100.94	--	25.74	--	Shear Failure
C-70RS	70	Stud	1120.69	+1.79%	33.05	+28.40%	Shear Failure
C-100S	100	Stud	1107.96	--	31.65	--	Shear Failure
C-100RS	100	Stud	1145.98	+3.43%	36.78	+16.21%	Shear Failure
C-50Y	50	Y-rib	1103.45	--	50	--	Shear Failure
C-50RY	50	Y-rib	1102.37	-0.1%	50	0.0	Shear Failure
C-70Y	70	Y-rib	1125.99	--	50	--	Shear Failure
C-70RY	70	Y-rib	1123.94	-0.18%	50	0.0	Shear Failure
C-100Y	100	Y-rib	1143.58	--	50	--	Shear Failure
C-100RY	100	Y-rib	1138.93	-0.41%	50	0.0	Shear Failure

*This is the ratio of the ultimate load of beams relative to the control beam without web opening (studs and Y-rib connections), (+) means increase (%) in the above properties with respect to reference beam, (-) means decrease (%) in the above properties.

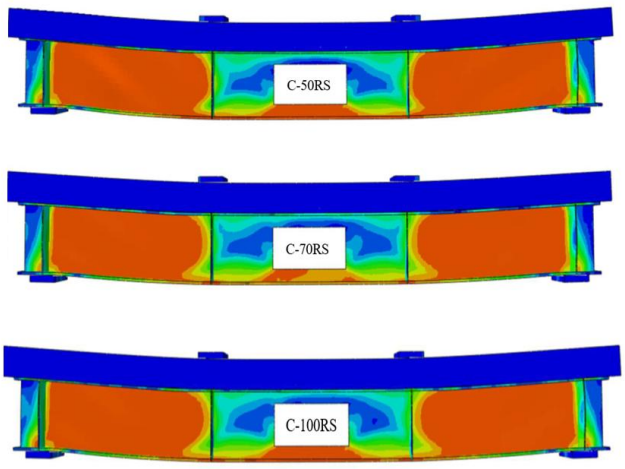

Figure 25. Crack patterns and mode of failure for opening bolt studs composite beams

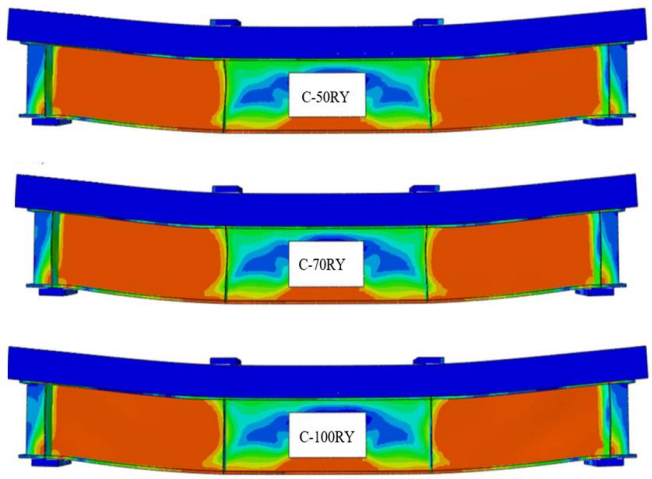

Figure 26. Crack patterns and mode of failure for opening Y-rib composite beams

5. BOND SLIP

The slip recorded in this study is the relative longitudinal displacement between the steel beam and the concrete slab and therefore directly measures how effectively shear connectors transfer longitudinal shear (interface shear flow) between the two components. When shear transfer is perfect (no slip) the section acts as a transformed, fully composite member and the internal bending moment is shared according to the transformed section stiffness. Any bond slip reduces that composite action: it lowers the effective flexural stiffness, concentrates additional demand on nearby connectors, increases curvature and mid-span deflection, and changes where and how cracks develop in the slab. In short, bond slip is a local mechanism with global consequences — it controls serviceability (deflections and crack widths), alters load distribution among components, and can either precipitate a brittle, connector-dominated failure or permit a more ductile redistribution depending on the connector system and its capacity.

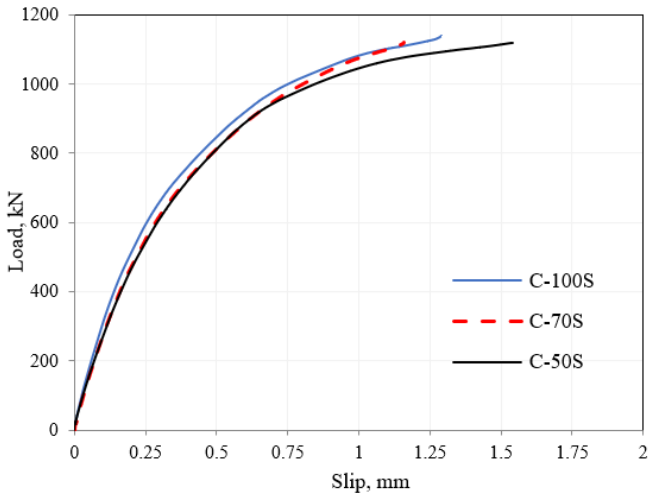

Figure 27. Load-slip relationship of bolt studs composite beam

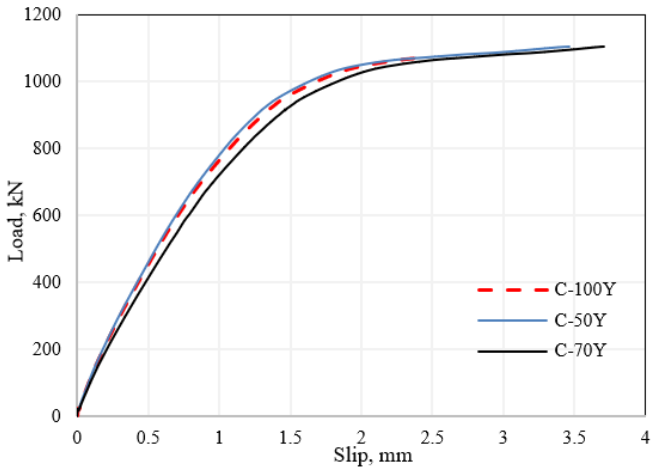

Figure 28. Load-slip relationship of composite beam

Figure 19's load–slip curves show these effects in microcosm. All specimens follow a similar, near-linear branch at small loads where slip is small and the connectors behave elastically; as load increases the interface demand grows and slip accelerates. The rapid rise of slip concurrent with the peak load (and the subsequent load drop) indicates that connector demand has exceeded local capacity (connector shear, concrete bearing, or interface bond) and the composite action is being lost. Figures 27 and 28 summarize the end-of-test slips at the same applied load level across the test matrix: for the stud series C-50S, C-70S, C-100S the slips were 1.54 mm, 1.16 mm and 1.29 mm respectively; for the Y-rib series C-50Y, C-70Y and C-100Y the slips were 3.46 mm, 3.71 mm and 3.09 mm respectively.

Two immediate patterns emerge from those numbers and the full load–slip traces. First, increasing the shear-connection ratio generally reduces slip in stud-connected beams: the 70% stud case (C-70S) shows lower slip than 50% (C-50S), indicating improved stiffness and load sharing as more connectors participate. The modestly higher slip in C-100S compared with C-70S is likely due to test-to-test scatter and to the fact that when connector density is high, other mechanisms (local concrete crushing, redistribution into the steel, or small differences in material properties and welding) can begin to govern so the simple monotonic trend is not always strictly linear in experimental data. Second, and more strikingly, the Y-rib specimens show substantially larger end slip values than the studs even though their load capacity and stiffness (from the load–deflection curves) are superior. Y-ribs give larger measured slips while still performing better overall. The explanation lies in how slip is generated and measured and in the qualitative difference between a discrete, point-wise connector system and a distributed, continuous connector. Discrete studs concentrate shear transfer at discrete points. Up to a certain load they behave very stiffly (small local slip), and then when local capacity is reached, they tend to produce abrupt, localized damage (radial cracks, stud shear/pull-out) and a sudden reduction in load transfer capacity. Y-ribs, by contrast, distribute shear transfer over a wider length and area. Rather than one or two studs taking most of the demand and then sharply failing, the Y-rib engages many micro-paths for shear flow and therefore deforms over a larger zone. That means: the local peak bearing and tensile stresses at any one point are reduced, so local crushing or stud pull-out is delayed. Further, the shear displacement is spread out over a longer interface length and so the measured end slip accumulates more gradually and over a greater total magnitude. Also, the load–slip curve is smoother and less abrupt, allowing the member to sustain and redistribute loads after cracking, shifting ultimate behaviour toward ductile flexural failure (steel yielding or compression-zone crushing) rather than brittle connector failure.

Thus, a higher measured end slip for Y-ribs does not necessarily indicate poorer performance. Instead, it reflects a higher slip capacity and a more benign, distributed deformation pattern. Where studs show small slip until a local limit is reached and then sudden loss, Y-ribs allow larger, controlled slip while maintaining load transfer and delaying catastrophic loss of composite action. This behaviour explains why Y-rib specimens returned higher ultimate loads and better post-cracking stiffness even though their numeric slip values at a given load were larger. Mechanically, bond slip affects ductility in two competing ways. If slip is highly localized and leads to early connector failure, the beam can lose stiffness abruptly and display reduced ductility (sudden loss of capacity). If slip is distributed and the connector system has reserve deformation capacity (as with Y-ribs), the structure can exhibit greater overall ductility: The load can be sustained as internal forces redistribute and plastic mechanisms develop

in the steel and concrete compression zone. This explains the paradox of higher slip but better global ductility and higher ultimate load in Y-rib specimens.

6. CONCLUSIONS

A numerical investigation into the response of a composite concrete beam encasing steel girder under static loads was presented. For this purpose, twelve specimens made with different types of shear connectors were considered. Two variables were considered in the numerical tests, including the types of shear connectors and the web opening. The following conclusion can be drawn from the present study:

- Increasing the shear connection ratio from 50% to 100% reduced measured slip values and increased stiffness in stud-connected beams, with the lowest slip recorded for C-70S (1.16 mm) and the highest for C-50S (1.54 mm).
- Y-rib connectors exhibited larger end slip values than studs at the same connection ratio (e.g., C-70Y: 3.71 mm vs. C-70S: 1.16 mm) but achieved higher ultimate loads and sustained composite action longer, indicating superior load redistribution and ductility.
- For beams with rectangular web openings, Y-rib strengthening reduced stress concentrations around the opening corners, delayed diagonal crack initiation, and shifted the governing failure mode from mixed flexural–shear to ductile flexural failure.
- Load–deflection results showed that Y-rib beams had a steeper initial stiffness and higher load capacity than stud beams, particularly in specimens with openings, due to more uniform shear transfer across the interface.
- Crack patterns observed experimentally matched the high tensile stress regions predicted in finite-element simulations, validating the numerical model's ability to identify crack initiation zones and predict failure modes.
- The combined experimental and numerical findings support the use of Y-rib connectors in applications requiring high load capacity, improved ductility, and better crack control, such as long-span composite floors and bridge decks.
- Future research should investigate the fatigue performance, durability under repeated loading, and seismic behaviour of Y-rib connections, as well as their performance in varying connector layouts and slab reinforcement ratios.

REFERENCES

[1] Shamass, R., Cashell, K.A. (2017). Behaviour of composite beams made using high strength steel. Structures, 12: 88-101. https://doi.org/10.1016/j.istruc.2017.08.005

[2] Mansour, F.R., Bakar, S.A., Ibrahim, I.S., Marsono, A.K., Marabi, B. (2015). Flexural performance of a precast concrete slab with steel fiber concrete topping. Construction and Building Materials, 75: 112-120. https://doi.org/10.1016/j.conbuildmat.2014.09.112

[3] Al-Rekabi, A.H., Daheer, M.A. (2024). Performance of sustainable fiber reinforced concrete with recycled aggregates: A critical review. AIP Conference Proceedings, 3079(1): 060014. https://doi.org/10.1063/5.0202348

[4] Ali, D.Y., Mahmood, R.A. (2024). Influence of slenderness ratio and sectional geometry on the behavior of steel braced frames. Engineering, Technology & Applied Science Research, 14(3): 14282-14286. https://doi.org/10.48084/etasr.7314

[5] Shariati, A., Sulong, N.H., Suhatril, M., Shariati, M. (2012). Investigation of channel shear connectors for composite concrete and steel T-beam. International Journal of the Physical Sciences, 7(11): 1828-1831. https://doi.org/10.5897/ijps11.1604

[6] Ollgaard, J.G., Slutter, R.G., Fisher, J.W. (1971). Shear strength of stud connectors in lightweight and normal-weight concrete. Engineering Journal, 8(2): 55-64. https://doi.org/10.62913/engj.v8i2.160

[7] Oehlers, D.J., Coughlan, C.G. (1986). The shear stiffness of stud shear connections in composite beams. Journal of Constructional Steel Research, 6(4): 273-284. https://doi.org/10.1016/0143-974X(86)90008-8

[8] Shim, C.S., Lee, P.G., Yoon, T.Y. (2004). Static behavior of large stud shear connectors. Engineering Structures, 26(12): 1853-1860. https://doi.org/10.1016/j.engstruct.2004.07.011

[9] Mirza, O., Uy, B. (2009). Behaviour of headed stud shear connectors for composite steel-concrete beams at elevated temperatures. Journal of Constructional Steel Research, 65(3): 662-674. https://doi.org/10.1016/j.jcsr.2008.03.008

[10] Shiyapov, K., Baishemirov, Z., Zhanbyrbayev, A. (2024). Advanced mathematical modelling of leaching processes in porous media: An averaging approach. Mathematical Modelling of Engineering Problems, 11(1): 151-158. https://doi.org/10.18280/mmep.110116

[11] Marshall, W.T., Nelson, H.M., Banerjee, H.K. (1971). An experiment study of the use of high-strength friction grip bolts as shear connectors in composite beams. Structural Engineer. 49(4): 171-178.

[12] Kwon, G., Engelhardt, M.D., Klingner, R.E. (2010). Behavior of post-installed shear connectors under static and fatigue loading. Journal of Constructional Steel Research, 66(4): 532-541. https://doi.org/10.1016/j.jcsr.2009.09.012

[13] Kwon, G., Engelhardt, M.D., Klingner, R.E. (2011). Experimental behavior of bridge beams retrofitted with postinstalled shear connectors. Journal of Bridge Engineering, 16(4): 536-545. https://doi.org/10.1061/(ASCE)BE.1943-5592.0000184

[14] Lam, D., Saveri, E. (2012). Shear capacity of demountable shear connectors. In Proceedings of the 10th International Conference on Advances in Steel Concrete Composite and Hybrid Structures, Singapore. https://doi.org/10.3850/978-981-07-2615-7_110

[15] Pavlović, M., Marković, Z., Veljković, M., Buđevac, D. (2013). Bolted shear connectors vs. headed studs behaviour in push-out tests. Journal of Constructional Steel Research, 88: 134-149. https://doi.org/10.1016/j.jcsr.2013.05.003

[16] Moynihan, M.C., Allwood, J.M. (2014). Viability and performance of demountable composite connectors. Journal of Constructional Steel Research, 99: 47-56. https://doi.org/10.1016/j.jcsr.2014.03.008

[17] Mirza, O., Uy, B., Patel, N. (2010). Behavior and strength of shear connectors utilising blind bolting. In

Steel and Composite Structures: Proceedings of the 4th International Conference on Steel and Composite Structures, Sydney, Australia, pp. 21-23. https://doi.org/10.3850/978-981-08-6218-3_SUS-Th022
[18] Darwin, D., Donahey, R.C. (1988). Design of composite beams with rectangular web openings. Journal of Structural Engineering, 114(3): 535-552. https://doi.org/10.1061/(ASCE)0733-9445(1988)114:3(535)
[19] Liao, W.Y., Li, L.Q., Liu, D.W., Dai, B.H., Wang, C.X. (2018). Nonlinear FEM analysis on composite beams with web opening under negative bending moment. Tehnički Vjesnik, 25(5): 1546-1552. https://doi.org/10.17559/TV-20180626222438
[20] Ataei, A., Bradford, M.A., Liu, X.P. (2016) Experimental study of composite beams having a precast geopolymer concrete slab and deconstruct able bolted shear connectors. Engineering Structures, 114: 1-13. https://doi.org/10.1016/j.engstruct.2015.10.041
[21] Clawson, W.C., Darwin, D. (1982). Tests of composite beams with web openings. Journal of the Structural Division, 108(1): 145-162. https://doi.org/10.1061/JSDEAG.0005856
[22] Donahey, R.C., Darwin, D. (1988). Web openings in composite beams with ribbed slabs. Journal of Structural Engineering, 114(3): 518-534. https://doi.org/10.1061/(ASCE)0733-9445(1988)114:3(518)
[23] Redwood, R.G., Poumbouras, G. (1983). Tests of composite beams with web holes. Canadian Journal of Civil Engineering, 10(4): 713-721. https://doi.org/10.1139/l83-100
[24] Fahmy, E.H. (1996). Analysis of composite beams with rectangular web openings. Journal of Constructional Steel Research, 37(1): 47-62. https://doi.org/10.1016/0143-974X(95)00022-N
[25] Benitez, M.A., Darwin, D., Donahey, R.C. (1998). Deflections of composite beams with web openings. Journal of Structural Engineering, 124(10): 1139-1147. https://doi.org/10.1061/(ASCE)0733-9445(1998)124:10(1139)
[26] Park, J.W., Kim, C.H., Yang, S.C. (2003). Ultimate strength of ribbed slab composite beams with web openings. Journal of Structural Engineering, 129(6): 810-817. https://doi.org/10.1061/(ASCE)0733-9445(2003)129:6(810)
[27] Al-Rekabi, A.H., Abo Dhaheer, M.S. (2024). Flexural performance of sustainable hybrid fibre-reinforced SCC beams made of treated recycled aggregates. Journal of Building Pathology and Rehabilitation, 9(1): 33. https://doi.org/10.1007/s41024-023-00382-3
[28] Al-Rekabi, A.H., Al-Marmadi, S.M., Dhaheer, M.A., Al-Ramahee, M. (2023). Experimental investigation on sustainable fiber reinforced self-compacting concrete made with treated recycled aggregate. AIP Conference Proceedings, 2775(1): 020032. https://doi.org/10.1063/5.0140655
[29] Hagen, N.C., Larsen, P.K., Aalberg, A. (2009). Shear capacity of steel plate girders with large web openings, Part I: Modeling and simulations. Journal of Constructional Steel Research, 65(1): 142-150. https://doi.org/10.1016/j.jcsr.2008.03.014
[30] Hagen, N.C., Larsen, P.K. (2009). Shear capacity of steel plate girders with large web openings, Part II: Design guidelines. Journal of Constructional Steel Research, 65(1): 151-158. https://doi.org/10.1016/j.jcsr.2008.03.005
[31] Sheehan, T., Dai, X., Lam, D., Aggelopoulos, E., Lawson, M., Obiala, R. (2016). Experimental study on long spanning composite cellular beam under flexure and shear. Journal of Constructional Steel Research, 116: 40-54. https://doi.org/10.1016/j.jcsr.2015.08.047
[32] Ellobody, E., Young, B. (2015). Behaviour and design of composite beams with stiffened and unstiffened web openings. Advances in Structural Engineering, 18(6): 893-918. https://doi.org/10.1260/1369-4332.18.6.893
[33] Lawson, R.M., Chung, K.F., Price, A.M. (1992). Tests on composite beams with large web openings to justify existing design methods. Structural Engineer London, 70(1): 1-7.
[34] Redwood, R.G., Pournbouras, G. (1984). Analysis of composite beams with web openings. Journal of Structural Engineering, 110(9): 1949-1958. https://doi.org/10.1061/(ASCE)0733-9445(1984)110:9(1949)
[35] Clawson, W.C., Darwin, D. (1982). Strength of composite beams at web openings. Journal of the Structural Division, 108(3): 623-641. https://doi.org/10.1061/JSDEAG.0005907
[36] Chung, K.F., Lawson, R.M. (2001). Simplified design of composite beams with large web openings to Eurocode 4. Journal of Constructional Steel Research, 57(2): 135-164. https://doi.org/10.1016/S0143-974X(00)00011-0
[37] Li, L., Liao, W., Wang, J., Zhou, D. (2015). Behavior of continuous steel-concrete composite beams with web openings. International Journal of Steel Structures, 15(4): 989-997. https://doi.org/10.1007/s13296-015-1218-2
[38] Pan, B., Qian, K.M., Xie, H.M., Asundi, A. (2009). Two-dimensional digital image correlation for in-plane displacement and strain measurement: A review. Measurement Science and Technology, 20(6): 062001. https://doi.org/10.1088/0957-0233/20/6/062001
[39] Sarsam, K.F., Mohammed, M.H. (2014). Load-deflection behavior of hybrid beams containing reactive powder concrete and conventional concrete. Journal of Engineering and Sustainable Development, 18(3): 118-147.
[40] Yazıcı, H., Yiğiter, H., Aydın, S., Baradan, B. (2006). Autoclaved SIFCON with high volume class C fly ash binder phase. Cement and Concrete Research, 36(3): 481-486. https://doi.org/10.1016/j.cemconres.2005.10.002
[41] Vijayakumar, M., Kumar, P.D. (2017). Study on strength properties of SIFCON. International Research Journal of Engineering and Technology (IRJET), 4(1): 235-238.
[42] Massicotte, B., Elwi, A.E., MacGregor, J.G. (1990). Tension-stiffening model for planar reinforced concrete members. Journal of Structural Engineering, 116(11): 3039-3058. https://doi.org/10.1061/(ASCE)0733-9445(1990)116:11(3039)
[43] Zienkiewicz, O.C., Taylor, R.L. (2000). Volume 1—The basis. In the Finite Element Method. Butterworth-Heinemann, Oxford.
[44] Ghazaly, N.M. (2014). Applications of finite element stress analysis of heavy truck chassis: Survey and recent development. Journal of Mechanical Design and Vibration, 2(3): 69-73.
[45] Smith, J.C. (1991). Structural Steel Design: LRFD

Approach. John Wiley & Sons.
[46] Malm, R. (2006). Shear cracks in concrete structures subjected to in-plane stresses. Doctoral thesis, Royal Institute of Technology (KTH), Stockholm, Sweden.
[47] Eriksson, D., Gasch, T. (2010). FEM-modeling of reinforced concrete and verification of the concrete material models available in ABAQUS. Royal Institute of Technology, Stockholm, Sweden.
[48] Kwak, Y.K., Eberhard, M.O., Kim, W.S., Kim, J. (2002). Shear strength of steel fiber-reinforced concrete beams without stirrups. ACI Structural Journal, 99(4): 530-538.
[49] Thevendran, V., Shanmugam, N.E., Chen, S., Liew, J.R. (2000). Experimental study on steel–concrete composite beams curved in plan. Engineering Structures, 22(8): 877-889. https://doi.org/10.1016/S0141-0296(99)00046-2
[50] Sika Corporation. (2023). SikaWrap®-300 C: Woven unidirectional carbon fibre fabric for structural strengthening applications. Version 01.03. Sika Corporation. https://gcc.sika.com/content/dam/dms/gcc/8/sikawrap_-300_c.pdf.
[51] Afazov, S.M., Becker, A.A., Hyde, T.H. (2012). Mathematical modeling and implementation of residual stress mapping from microscale to macroscale finite element models. Journal of Manufacturing Science and Engineering, 134(2): 021001. https://doi.org/10.1115/1.4006090
[52] Li, L., Zhang, H., Zhou, D. (2021). Experimental study of high-strength bolt connected composite beams with web openings. Iranian Journal of Science and Technology, Transactions of Civil Engineering, 45(1): 1-10. https://doi.org/10.1007/s40996-020-00411-y